SCIENTIFIC REPORTS

OPEN

SUBJECT AREAS:
NANOCOMPOSITES
METAL-ORGANIC FRAMEWORKS

Received
12 October 2014

Accepted
11 December 2014

Published
16 January 2015

Correspondence and requests for materials should be addressed to S.J.D.S. (stefan.smith@monash.edu) or M.R.H. (matthew.hill@csiro.au)

Post-synthetic Ti Exchanged UiO-66 Metal-Organic Frameworks that Deliver Exceptional Gas Permeability in Mixed Matrix Membranes

Stefan J. D. Smith[1,2], Bradley P. Ladewig[1], Anita J. Hill[2], Cher Hon Lau[2] & Matthew R. Hill[2]

[1]Monash University, Department of Chemical Engineering, Clayton, VIC 3800, Australia, [2]CSIRO, Private Bag 33, Clayton South MDC, VIC 3169, Australia.

Gas separation membranes are one of the lowest energy technologies available for the separation of carbon dioxide from flue gas. Key to handling the immense scale of this separation is maximised membrane permeability at sufficient selectivity for CO_2 over N_2. For the first time it is revealed that metals can be post-synthetically exchanged in MOFs to drastically enhance gas transport performance in membranes. Ti-exchanged UiO-66 MOFs have been found to triple the gas permeability without a loss in selectivity due to several effects that include increased affinity for CO_2 and stronger interactions between the polymer matrix and the Ti-MOFs. As a result, it is also shown that MOFs optimized in previous works for batch-wise adsorption applications can be applied to membranes, which have lower demands on material quantities. These membranes exhibit exceptional CO_2 permeability enhancement of as much as 153% when compared to the non-exchanged UiO-66 mixed-matrix controls, which places them well above the Robeson upper bound at just a 5 wt.% loading. The fact that maximum permeability enhancement occurs at such low loadings, significantly less than the optimum for other MMMs, is a major advantage in large-scale application due to the more attainable quantities of MOF needed.

Combustion of coal accounts for 41% of electricity generation globally, contributing 8270 million tonnes to annual anthropogenic carbon dioxide emissions[1,2]. As a consequence; technologies that can isolate carbon dioxide from the exhaust stream are relevant (known as post-combustion capture, PCC). One of the key challenges for prospective carbon capture technologies is the energy required to operate the process. Batch-wise technologies that rely on temperature, pressure or vacuum swing processes to regenerate materials employed for carbon dioxide capture can require significant proportions of the power plant's produced energy for this operation[1]. As a consequence, continuous processes that offer lower energy demands are attractive for further investigation.

Membranes are prospective alternatives that operate through the transport of gases at varying rates through the thin selective membrane layer. In this case, carbon dioxide can pass through the membrane layer significantly faster than nitrogen, the predominant gas in the flue stream. Assessments for the required operating performances of gas separation membranes in PCC setting are that a membrane must have a selectivity for CO_2 over N_2 of at least 20 to sufficiently concentrate the product for sequestration or utilisation, and, having attained this, operate with maximum CO_2 permeability due to the diminishing savings in energy costs at higher selectivities, and the sheer scale of the task at hand[3–5]. The most readily processible membranes are polymer-based systems, yet, as originally described by Robeson and explained by Freeman[6–8], there is a trade-off between these two target attributes of permeability and selectivity, largely as a result of the limited control attainable between the number and size of pores within polymer films.

Within this set of materials, polymers of intrinsic microporosity (PIMs) are attractive candidates[9–11]. Since their inception in the early 2000s, PIMs have found applications ranging from separating gases and liquids[12] to polymer resists[13]. Consisting of contorted spirobisindane and dioxane units, PIM-1 exhibits both high selectivity and permeability for the CO_2/N_2 gas pair[11,14]. Additionally, the nitrile groups in PIM-1 can be functionalised to tailor membrane properties to suit application requirements[13,15–18].

Recently, we showed that the porous additive PAF-1 can be used to intercalate with the side chains of the polymer, stopping physical aging within the membrane[19]. A promising approach for improving polymeric membranes is to add filler particles, forming mixed matrix membranes (MMMs)[20–22]. Inorganic fillers such as SiO_2[23–25] or TiO_2[26–29] have been widely explored, and depending on particle agglomeration, can drastically enhance gas transport and separation properties of MMMs. However, owing to the additional gas transport pathways through the pores of porous materials, the incorporation of porous materials into polymer matrices can improve gas transport and separation properties better than their non-porous analogues (Figure 1)[30–32]. Unfortunately, high particle content is usually required to generate optimal separation enhancement, which impacts application costs and can compromise mechanical durability of the composite.

Metal Organic Frameworks (MOFs) are metal atoms or clusters connected periodically to one another by organic linker units. Their regular pores, lined with under-coordinated, polarising metal atoms, are ripe for selective gas transport. Additionally, record breaking internal surface areas, which are in well-interconnected porous architectures, offer rapid gas transport pathways; and are known to improve the gas permeability and selectivity of polymer membranes. Sivaniah and co-workers reported that the inclusion of 30 wt.% ZIF-8 nanoparticles into Matrimid®, a commercially available polyimide, can enhance gas permeability with negligible losses in selectivity through the increase in free volume of polymer with ZIF-8 loading and the free diffusion of gas through the cages of ZIF-8[33]. Musselman and co-workers incorporated 50 wt.% ZIF-8 in Matrimid®, and improved the ideal gas selectivities of such nanocomposites, at the expense of gas permeabilities; demonstrating a transition from a polymer-driven to a MOF controlled gas transport process[34]. Yang and Chung demonstrated that ZIF-8/polybenzimidazole nanocomposites exhibited remarkably high mixed gas selectivities at high temperatures, and the presence of CO and water did not impact H_2/CO_2 separation[35]. These recent works show that MOF-loaded MMMs improve gas permeabilities *via* the provision of open gas transport channels, formation of additional free volume elements at the interface between polymer and nanoparticle, and through high loadings of MOF that provide a direct pathway for gas transport.

A possible route to further improve the gas transport properties of MOF-loaded MMMs is to utilise enhanced gas uptakes of MOFs with functionalised linkers[36]. We have expanded this investigation to also examine the effect of metal exchange[37]. Recently, it was reported that one of the few water and high temperature stable MOFs, the Zr-based UiO-66, can be post-synthetically exchanged with titanium[38]. In our previous work, the smaller Ti atom was found to shrink the pores within the framework, which, in concert with the improved size-to-charge ratio of Ti^{4+} for polarising CO_2, delivered drastically enhanced adsorption capacity[39]. Additionally, the exchanged "Ti_xUiO-66", where 'x' is the metal exchange incubation period (days), maintains UiO-66's very high thermal and chemical stability[40] as well as its structural stability through water adsorption/desorption cycles[41].

Described herein is the systematic post-synthetic transmetallation of Ti^{IV} ions into the Zr UiO-66 framework to deliver remarkable increases in separation performance, placing the resulting mixed matrix membranes well above the Robeson upper bound[7]. The rate of membrane aging was also reduced. Preparation and characterisation of the films as a function of MOF loading and Ti-exchange period allowed for the factors behind the exceptional performance to be deduced.

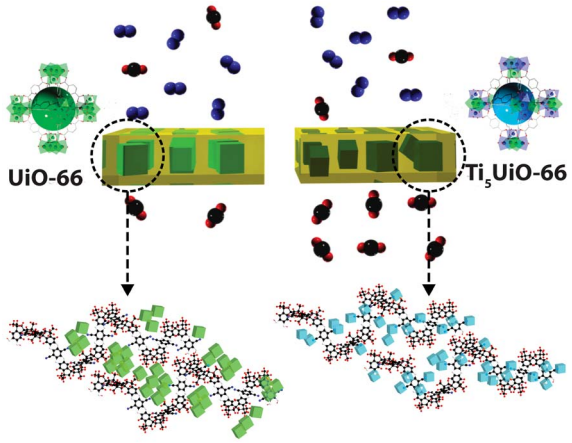

Figure 1 | Ti-exchange of UiO-66 MOF increases the interaction with PIM-1 polymer, leading to a drastic increase in CO_2 permeability in comparison to a UiO-66 PIM-1 membrane.

Results

As hypothesised, addition of the Ti_xUiO-66 into PIM-1 resulted in a drastic increase in CO_2 permeability, with the greatest measured result (Ti_5, 5 wt.%, 13500 Barrer) 274% higher than that of the pristine PIM-1 membrane (denoted as 0 wt.% loading in Figure 2). This permeability is also 153% higher than the corresponding native UiO-66 mixed matrix membrane (5340 Barrer), confirming the titanium exchange further improved separation performance. Membranes containing Ti exchanged UiO-66 exhibit a rapid increase in permeability at low loadings, which offers a competitive advantage over other reported MMMs[23–25,42,43] that exhibited maximum permeability when loadings approached 50 wt.%. The large increase in permeability effect can be isolated as being particular to Ti-substitution. Ideal selectivities were unaffected by the level of titanium exchange and also MOF loading levels (Table S3†). The higher gas adsorption and stronger CO_2 affinity in Ti-exchanged MOFs (Table 1) did not influence the level of selective gas transport.

The polymer-MOF interactions were interrogated with DSC analysis (Figure 3), which showed that Ti_xUiO-66 membranes had higher peak decomposition temperatures than the similarly loaded native UiO-66 membranes (Figures S17, S18†). The increased decomposition temperature of Ti_xUiO-66 membrane suggests that the Ti exchange of UiO-66 affects the MOF's exterior surface, resulting in a stronger polymer-MOF interaction and increased thermal stability.

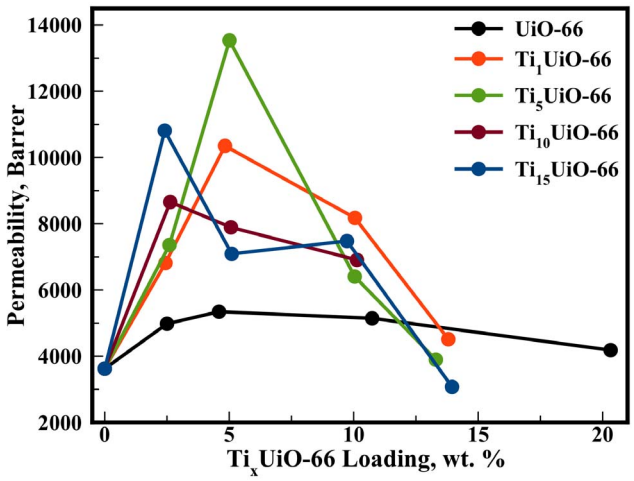

Figure 2 | CO_2 Permeability of PIM-1 Ti_xUiO-66 mixed matrix membranes. Permeability measurement recorded with a pressure differential of 2 Bar, at 298 K and within +/− 5% deviation. (ESI-10†). Lines are drawn to guide the eye.

Table 1 | Brunauer-Emmett-Teller (BET) and Langmuir surface area

Ti_xUiO-66	BET surface Area[a], m^2/g	Langmuir surface area[a], m^2/g	CO_2 adsorption[b], mmol/g (STP)
UiO-66	1263	1471	2.53
Ti_1UiO-66	1263	1482	2.83
Ti_5UiO-66	1359	1535	3.06
Ti_{10}UiO-66	1328	1487	3.07
Ti_{15}UiO-66	1249	1448	2.83

[a]calculations based on N_2 isotherm data measured at 77 K.
[b]maximum CO_2 adsorption measured at 273 K and 1.2 Bar.

This increased polymer-MOF interaction was confirmed by viscosity measurements of the 5 wt.% membrane casting solutions (Figure 4) that showed solution viscosity decreases with increasing Ti exchange.

Changes in viscosity can be used to identify the various interactions in composite materials. There are three main interactions that can lead to a lowering of viscosity:

(a) reduction of polymer entanglement by surface absorption to the additive[41]
(b) increase in free volume[42,43]
(c) confinement with the additive's pores[44]

The significant drop in viscosity with the addition of UiO-66 may be assigned to the increased free volume as confirmed by density measurements (Figure S20). Further drops for Ti_5 and Ti_{15} samples must come from (a) *surface absorption* as their free volume was actually lower (Figure S20), and (c) *confinement* identical in all MOF additions due to their isomorphism. As a consequence this directly confirms that Ti-transmetallation delivers a stronger MOF-polymer interaction. Interaction of PIM-1's nucleophillic groups occurs with exposed Ti^{IV}/Zr^{IV} metal sites, which increases with the loss of crystallinity caused by Ti substitution (Figure S12†).

SEM images of PIM-1 Ti_5UiO-66 membranes (Figure 5) exhibit surface topologies similar to previously reported mixed matrix membranes[23,34,42,44], characteristic of particle interaction at the polymer interface. Images also reveal agglomeration of Ti_xUiO-66 MOF at higher loadings, which increases effective particle size.

The different CO_2 permeability, solubility and diffusivity values in Table 2 can be attributed to the different PIM-1 synthesis protocol adopted in this work. The depressed solubility coefficients in MOF-loaded membranes increase with Ti-incorporation. As predicted by Cohen and Turnbull's Free Volume theory, the permeability enhancement was largely generated by the increase in diffusivity coefficient (Table 2, right)[45]. Notably, the titanium exchange in the Ti_5UiO-66 (5 wt.%) membrane significantly improved both the solubility (+23%) and diffusivity coefficients (+106%) over the corresponding native UiO-66 membrane.

As depicted in Figure 6, the permeability trends measured across the series of mixed matrix membranes are best described as the result of an additive effect between several competing factors. Permeability enhancements are assigned to the effects of increased CO_2 sorption and diffusion in MOFs (**a**–**b**, at low loadings) and higher free volume within PIM-1 (**c**). Losses in permeability relate to lower CO_2 MOF diffusion and PIM-1 fractional free volume (**b**, high loadings) and also the lower MOF crystallinity in Ti-substituted MOFs (**d**). Permeability enhancement factors **a**, **b** and **c** are accentuated by the Ti MOF substitution compared to the Zr MOF counterparts, accounting for the drastic increase in CO_2 permeability with Ti-substitution in MOFs. The lower CO_2 permeability in high loading Ti-substituted MOF membranes compared to PIM-1 controls is related to the lower crystallinity resulting from Ti-substitution in the Zr-MOF UiO-66.

CO_2 sorption (**a**) was found to increase as shown in Table 1, dropping away with increased Ti loading. This aligns with values previously reported[38,39]. CO_2 diffusivity (**b**) was by far the strongest effect, accounting for the beneficial enhancement of CO_2 permeability. Diffusivity increased by a factor of four in Ti substituted MOF samples and by a factor of 2 in the Zr analogues. Free volume in PIM-1 (**c**) is affected by the well known increase in polymer free volume (Figure S9†) upon nanoparticle addition[23,24,45], which is eventually decreased with strong polymer-MOF interactions occurring. These interactions are witnessed in the stabilisation of membranes during DSC (Figure S18†) when Ti is introduced, the reduction of viscosity of PIM-1 Ti_xUiO-66 solutions with increasing Ti (Figure S26†), and the lower level of MOF agglomeration in SEM (Figures S21-S25†). The

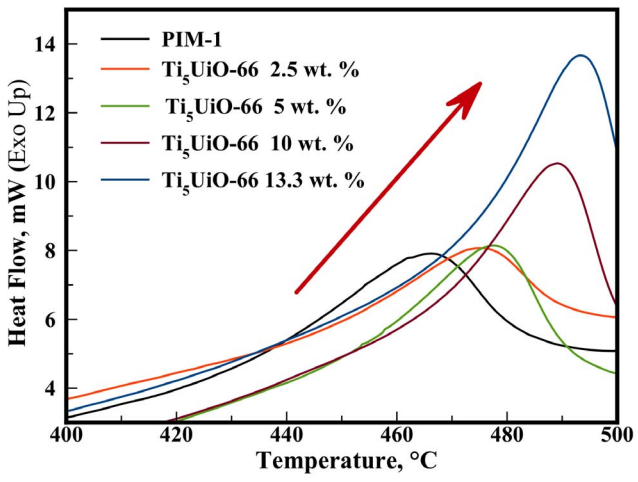

Figure 3 | DSC analysis of the PIM-1 Ti_5UiO-66 membranes. Arrow highlights the trend in peak decomposition.

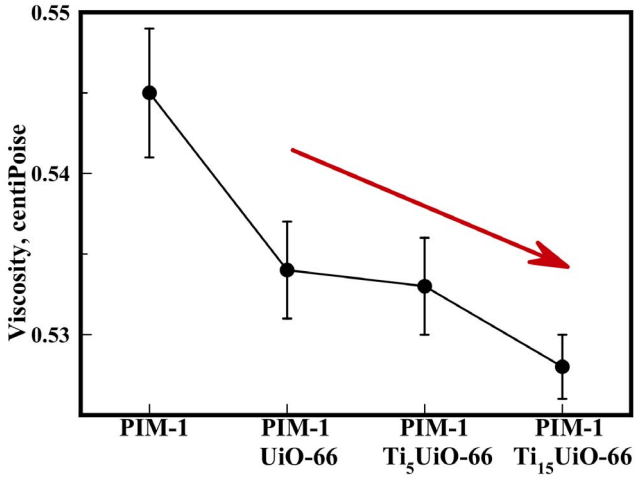

Figure 4 | Viscosity of Aged PIM-1 Ti_xUiO-66 (5 wt.%) membrane casting solutions (Table S6†). Arrow highlights trend in viscosity. Line drawn to guide the eye.

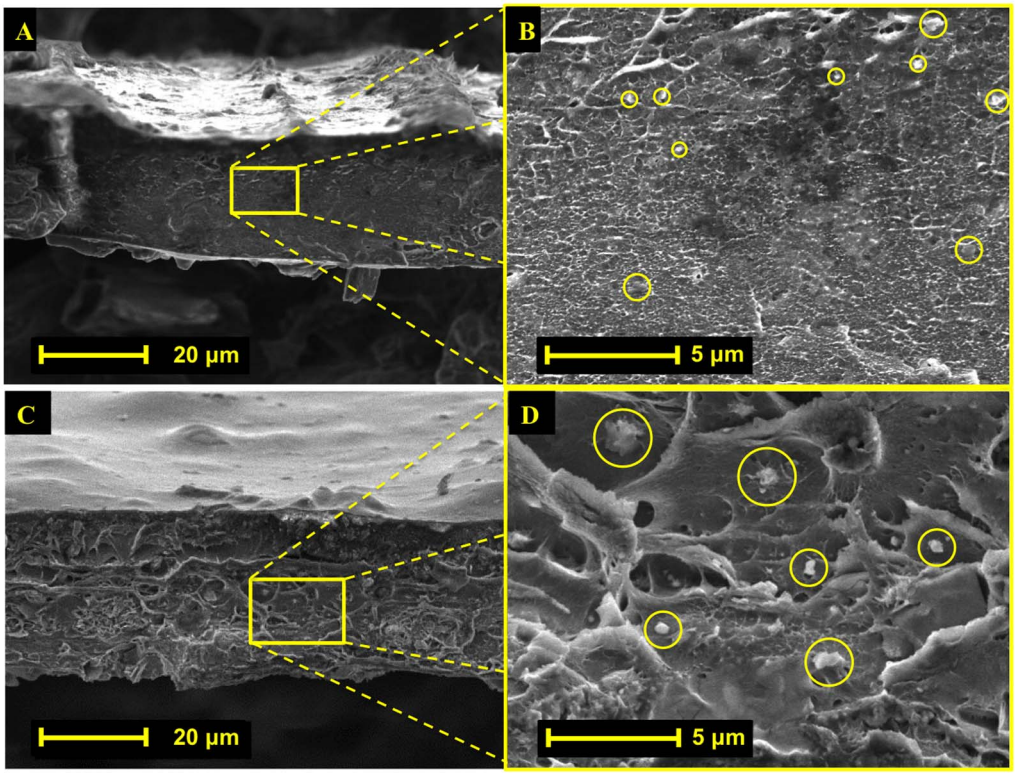

Figure 5 | **Cross sectional SEM images of PIM-1 Ti_5UiO-66 membranes 2.6 wt.% (A, B) and 15 wt.% (C, D), respectively.** Highlighted regions of (A, C) are shown at higher magnification to identify MOF locations in images (B, D), respectively.

enhanced exposure and reactivity of Ti-exchanged SBUs is a likely contributor to this strengthened polymer-MOF interaction[39,46–50]. MOF crystallinity clearly diminishes with the level of Ti substitution, as seen in broadening PXRD peaks (Figure S12†)[38,51]. This is in agreement with our previous findings[39] and leads to fewer ordered gas transport pathways through the MOF.

Taken together, the factors measured within this present study reveal that the mechanism responsible for the remarkable gas transport properties recorded is an additive combination of several structural and chemical changes that are as a result of both the loading of MOFs into the PIM-1 polymer membrane, and the titanium substitution within the MOF additives.

Another factor affecting the industrial application of membranes is their useable lifetime. Inclusion of Ti_5UiO-66 (5 wt.%) nanoparticles resulted in a significant increase in gas permeability, and also decreased the rate of relative permeability loss in the PIM-1 membranes over time (Figure 7). Notably, CO_2/N_2 ideal selectivity increased (α = 20 to 24) in both membranes over the course of membrane aging. Loading of 5 wt.% Ti_5UiO-66 also improved the PIM-1's mechanical properties under 2 Bar of gas pressure, not exhibiting any instance of mechanical failure under testing conditions for 63 days, compared to pristine PIM-1's consistent membrane fracture after 24 days of aging. This indicated improved mechanical stability in the MOF composite membranes.

Discussion

This work reports the study of the gas permeation performance of mixed matrix membranes developed specifically for improving CO_2/N_2 separation performance for the application of carbon capture and sequestration. The hypothesised amalgamation of PIM-1, a polymer already near the Robeson upper bound, and a previously demonstrated MOF of high CO_2 affinity, Ti-exchanged UiO-66, generated a significant increase in membrane CO_2 permeability (13500 Barrer, +274%). This improvement was achieved without selectivity loss, exceeding the CO_2/N_2 Robeson Upper bound (Figure 8) and the separation performance of a number of other high performance mixed matrix membranes. This study highlights the potential advantages of matching materials and tuning the surface of nanoparticles in polymeric mixed matrix membranes. The strong interaction between Ti_xUiO-66's exposed metal centres to PIM-1 polymer has significant effects on the formation of interfacial free volume, generating a significant increase in permeability at the optimal loading of 5 wt.%, a loading significantly lower than peak performance of other MMM's (40–60%). This study also provides a validation for research

Table 2 | Permeability (P), Solubility (S) and Diffusivity (D) Coefficients

Membrane	P (CO_2)	S (1 atm, 298 K)	D
	Barrer	cm^3(STP)/cm^3atm	x10^5 cm^2s^{-1}
PIM-1	3620	41.8	0.07
PIM-1 UiO-66 5 wt.%	5340	26.2	0.16
PIM-1 Ti_5UiO-66 5 wt.%	13540	32.3	0.32

Diffusivity coefficients were calculated from Permeability data and Solubility coefficients (1 atm). Dual mode sorption parameters were derived from CO_2 sorption measurements (Refer ESI-15†).

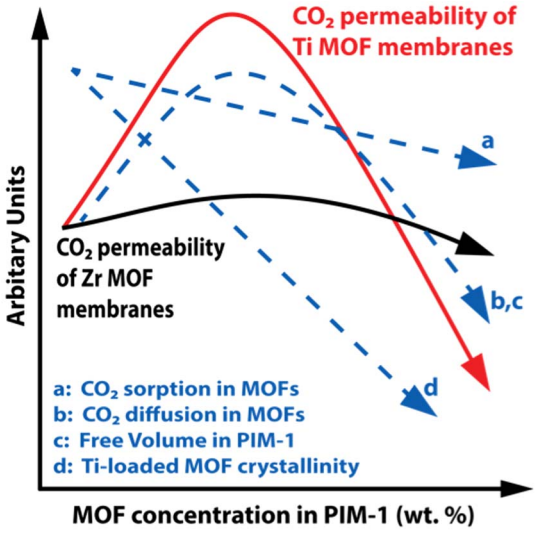

Figure 6 | Summary of deterministic effects that influence CO_2 permeability in PIM-1 membranes studied here.

involving transmetallation of MOFs as a route to further improve mixed matrix membrane performance.

Methods

Synthesis of PIM-1. The synthesis of PIM-1 polymer is based on a rapid polycondensation reaction of 2,3,5,6-Tetrafluoroterephthalonitrile (TFTPN) (12.5 mmol) and 5,5′,6,6′-tetrahydroxy-3,3,3′,3′-tetramethyl-1,1-spirobisindane (TTSBI) (12.7 mmol) in the presence of excess anhydrous K_2CO_3 (38.8 mmol), however a previously unreported solvent mixture of DMAc (25 mL) and CS_2 (12.5 mL) was used[15,52,53]. The reaction mixture (under inert atmosphere) was refluxed using a dean stark trap at 165°C. for an hour. The reaction solution was decanted into stirred MeOH to precipitate the polymer. The product was then dissolved in $CHCl_3$ and recrystallized from MeOH before being dried by vacuum filtration.

Synthesis of UiO-66. UiO-66 was prepared as previously reported[39,54]. Equimolar quantities (43 mmol) of zirconium tetrachloride and 1,4-benzenedicarboxylic acid were reacted in the presence of a large excess (684 mmol) of benzoic acid in a DMF:H_2O (1650:83 mL) solvent. The resulting product was washed sequentially with DMF and MeOH before being dried under vacuum at 100°C.

Post synthetic exchange of UiO-66 with Ti^{IV}. Titanium exchange of the UiO-66's Zirconium metal centres followed the recently reported method using $TiCl_4(THF)_2$ in DMF at 85°C[38,39]. Equimolar quantities (0.45 mmol) of $TiCl_4(THF)_2$ and synthesised UiO-66 were suspended in 10 mL DMF and incubated for a range of exchange periods (1, 5, 10, and 15 days). After cation exchange, Ti_xUiO66 samples were washed sequentially in DMF and MeOH before being vacuum dried at 100°C.

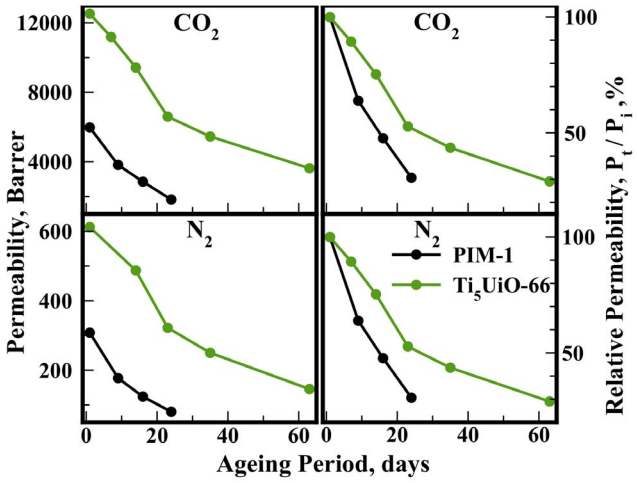

Figure 7 | Permeability of aged PIM-1 Ti_5UiO-66 (5 wt.%) and PIM-1 membranes. Stored in air between measurements. (Table S5†).

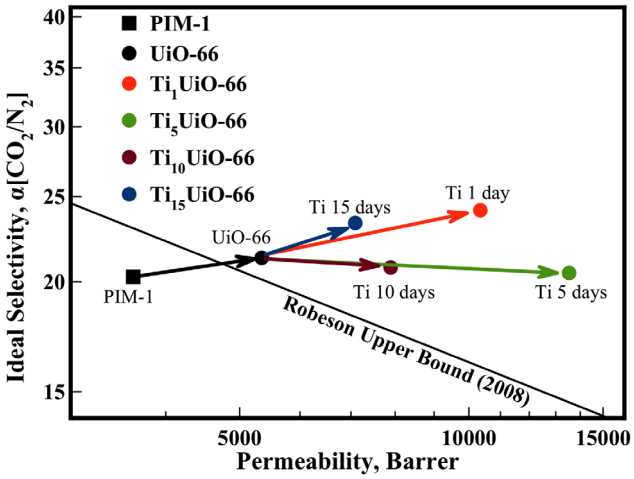

Figure 8 | PIM-1 Ti_xUiO-66 (5 wt.%) membranes plotted against the Robeson Upper Bound[7] (2008). Arrows highlight effect of UiO-66 inclusion and Ti exchange

Membrane Preparation. Membranes were cast at ambient conditions from ~0.2 g/mL $CHCl_3$ solutions in 75 mm diameter PTFE dishes, covered in perforated aluminium foil, and vacuum dried (80°C) overnight before use. Single gas (N_2, H_2, CH_4, and CO_2) permeation measurements were undertaken in duplicate on the day following casting to maintain a consistent processing history[11].

Characterisation. NMR spectra (^{13}C and ^{1}H) of the PIM-1 used in this study were recorded using a Bruker Av500 and Bruker Av400X, respectively. †). *Gel Permeation Chromatography (GPC) of the PIM-1 Polymer was completed in THF* (30°C flow rate: 1 mL min^{-1}) *using* Waters Alliance e2695 liquid chromatograph equipped with a Waters 2414 differential refractometer. Powder X-Ray Diffraction (PXRD) spectra were collected on a Bruker D8 Advance X-ray Diffractometer, using Cu K-alpha radiation (40 kV, 40 mA) equipped with a LynxEye silicon strip detector. Samples were scanned over the 2θ range 5° to 85° with a step size of 0.02° 2θ and a count time of 0.4 seconds per step. Adsorption isotherms of the prepared Titanium exchanged and native UiO-66 were measured using an ASAP 2420 with carbon dioxide (273 K, 298 K) and nitrogen (77 K, 273 K) adsorbates. MOF samples were activated at 120°C under vacuum overnight prior to analysis. Langmuir and BET surface areas were calculated from nitrogen isotherms at 77 K. Fourier-Transform Infrared (FTIR) spectroscopy was undertaken with a Thermo Scientific NICOLET 6700 FT-IR on the product PIM-1 polymer, the synthesis reactants, and the range of Ti_xUiO-66 used in the study. DSC measurements were made using a Mettler Toledo Differential Scanning Calorimeter. Samples were encapsulated in aluminium pans and heated from 25°C to 500°C at 10°C/min. Pycnometry measurements were made using an AccuPyc Pycnometer (He) to determine the relative density, and by extension, free volume present in the prepared Ti_xUiO-66 PIM-1 membranes. A Philips XL30 Field Emission Scanning Electron Microscope (FESEM) with an accelerating voltage of 5 kV was used for imaging the cross sectional surface of membrane samples (Figure S21-25†). Cross-section surfaces were prepared by fracturing membranes in liquid nitrogen and mounting to SEM stubs using carbon tape, before sputter coating with platinum. Membrane solubility coefficients were calculated from High-pressure Sorption (Setaram PCT Pro) measurements. Dual-mode sorption parameters were calculated by curve fitting to equation 1, as reported.[11] Viscosity measurements were made using a SCHOTT AV350 Viscometer (standard ASTM D445) using a 52610/I U-tube calibrated with a de-ionised water standard at 20°C.

1. Boot-Handford, M. *et al.* Carbon Capture and Storage Update. *Energ. Environ. Sci.* **7**, 130,189 (2013).
2. Anderson, S. & Newell, R. Prospects for carbon capture and storage technologies. *Annu. Rev. Environ. Resour.* **29**, 109–142 (2004).
3. Merkel, T. C., Lin, H., Wei, X. & Baker, R. Power plant post-combustion carbon dioxide capture: An opportunity for membranes. *J. Membr. Sci.* **359**, 126–139 (2010).
4. Koros, W. J. & Mahajan, R. Pushing the limits on possibilities for large scale gas separation: which strategies? *J. Membr. Sci.* **175**, 181–196 (2000).
5. Lively, R. P. *et al.* A high-flux polyimide hollow fiber membrane to minimize footprint and energy penalty for CO_2 recovery from flue gas. *J. Membr. Sci.* **423–424**, 302–313 (2012).
6. Robeson, L. M. Correlation of separation factor versus permeability for polymeric membranes. *J. Membr. Sci.* **62**, 165–185 (1991).
7. Robeson, L. M. The upper bound revisited. *J. Membr. Sci.* **320**, 390–400 (2008).

8. Freeman, B. D. Basis of Permeability/Selectivity Tradeoff Relations in Polymeric Gas Separation Membranes. *Macromolecules* **32**, 375–380 (1999).
9. McKeown, N. B. & Budd, P. M. Exploitation of Intrinsic Microporosity in Polymer-Based Materials. *Macromolecules* **43**, 5163–5176 (2010).
10. Budd, P. M. *et al.* Gas permeation parameters and other physicochemical properties of a polymer of intrinsic microporosity: Polybenzodioxane PIM-1. *J. Membr. Sci.* **325**, 851–860 (2008).
11. Li, P., Chung, T. S. & Paul, D. R. Gas sorption and permeation in PIM-1. *J. Membr. Sci.* **432**, 50–57 (2013).
12. Budd, P. M. *et al.* Solution-Processed, Organophilic Membrane Derived from a Polymer of Intrinsic Microporosity. *Adv. Mater.* **16**, 456–459 (2004).
13. Song, Q. *et al.* Photo-oxidative enhancement of polymeric molecular sieve membranes. *Nat. Commun.* **4**, 1918 (2013).
14. Budd, P. M. *et al.* Gas separation membranes from polymers of intrinsic microporosity. *J. Membr. Sci.* **251**, 263–269 (2005).
15. Du, N. *et al.* Polymers of Intrinsic Microporosity Containing Trifluoromethyl and Phenylsulfone Groups as Materials for Membrane Gas Separation†. *Macromolecules* **41**, 9656–9662 (2008).
16. Du, N., Robertson, G. P., Dal-Cin, M. M., Scoles, L. & Guiver, M. D. Polymers of intrinsic microporosity (PIMs) substituted with methyl tetrazole. *Polymer* **53**, 4367–4372 (2012).
17. Du, N., Dal-Cin, M. M., Robertson, G. P. & Guiver, M. D. Decarboxylation-Induced Cross-Linking of Polymers of Intrinsic Microporosity (PIMs) for Membrane Gas Separation†. *Macromolecules* **45**, 5134–5139 (2012).
18. Du, N. *et al.* Polymer nanosieve membranes for CO_2-capture applications. *Nat. Mater.* **10**, 372–375 (2011).
19. Lau, C. H. *et al.* Ending Aging in Super Glassy Polymer Membranes. *Angew. Chem. Int. Ed.* **53**, 5322–5326 (2014).
20. Tanh Jeazet, H. B., Staudt, C. & Janiak, C. Metal-organic frameworks in mixed-matrix membranes for gas separation. *Dalton Trans.* **41**, 14003–14027 (2012).
21. Kentish, S. E., Scholes, C. A. & Stevens, G. W. Carbon Dioxide Separation through Polymeric Membrane Systems for Flue Gas Applications. *Recent Pat. Chem. Eng.* **1**, 14 (2008).
22. Yao, J. & Wang, H. Zeolitic imidazolate framework composite membranes and thin films: synthesis and applications. *Chem. Soc. Rev.* **43**, 4470–4493 (2014).
23. Ahn, J. *et al.* Gas transport behavior of mixed-matrix membranes composed of silica nanoparticles in a polymer of intrinsic microporosity (PIM-1). *J. Membr. Sci.* **346**, 280-287 (2010).
24. Merkel, T. C. *et al.* Ultrapermeable, reverse-selective nanocomposite membranes. *Science* **296**, 519–522 (2002).
25. Mason, C. R. *et al.* New organophilic mixed matrix membranes derived from a polymer of intrinsic microporosity and silicalite-1. *Polymer* **54**, 2222–2230 (2013).
26. Roh, D. K., Kim, S. J., Jeon, H. & Kim, J. H. Nanocomposites with Graft Copolymer-Templated Mesoporous MgTiO Perovskite for CO Capture Applications. *ACS Appl. Mater. Interfaces* **5**, 6615–6621 (2013).
27. Hu, Q. *et al.* Poly(amide-imide)/TiO2 nano-composite gas separation membranes: Fabrication and characterization. *J. Membr. Sci.* **135**, 65–79 (1997).
28. Matteucci, S., Kusuma, V. A., Sanders, D., Swinnea, S. & Freeman, B. D. Gas transport in TiO2 nanoparticle-filled poly(1-trimethylsilyl-1-propyne). *J. Membr. Sci.* **307**, 196–217 (2008).
29. Madaeni, S. S., Badieh, M. M. S., Vatanpour, V. & Ghaemi, N. Effect of titanium dioxide nanoparticles on polydimethylsiloxane/polyethersulfone composite membranes for gas separation. *Polym. Eng. Sci.* **52**, 2664–2674 (2012).
30. Brown, A. J. *et al.* Continuous Polycrystalline Zeolitic Imidazolate Framework-90 Membranes on Polymeric Hollow Fibers. *Angew. Chem. Int. Ed.* **124**, 10767–10770 (2012).
31. Abedini, R., Omidkhah, M. & Dorosti, F. Highly permeable poly(4-methyl-1-pentyne)/NH2-MIL 53 (Al) mixed matrix membrane for CO_2/CH4 separation. *RSC Advances* **4**, 36522–36537 (2014).
32. Zornoza, B. *et al.* Functionalized flexible MOFs as fillers in mixed matrix membranes for highly selective separation of CO_2 from CH4 at elevated pressures. *Chem Commun (Camb)* **47**, 9522–9524 (2011).
33. Song, Q. *et al.* Zeolitic imidazolate framework (ZIF-8) based polymer nanocomposite membranes for gas separation. *Energ. Environ. Sci.* **5**, 8359–8369 (2012).
34. Ordoñez, M. J. C., Balkus Jr, K. J., Ferraris, J. P. & Musselman, I. H. Molecular sieving realized with ZIF-8/Matrimid® mixed-matrix membranes. *J. Membr. Sci.* **361**, 28–37 (2010).
35. Yang, T. & Chung, T.-S. High performance ZIF-8/PBI nano-composite membranes for high temperature hydrogen separation consisting of carbon monoxide and water vapor. *Int. J. Hydrogen Energ.* **38**, 229–239 (2013).
36. Zhang, Z., Zhao, Y., Gong, Q., Li, Z. & Li, J. MOFs for CO_2 capture and separation from flue gas mixtures: the effect of multifunctional sites on their adsorption capacity and selectivity. *Chem. Commun.* **49**, 653–661 (2013).
37. Takaishi, S., DeMarco, E. J., Pellin, M. J., Farha, O. K. & Hupp, J. T. Solvent-assisted linker exchange (SALE) and post-assembly metallation in porphyrinic metal-organic framework materials. *Chem. Sci.* **4**, 1509–1513 (2013).
38. Kim, M., Cahill, J. F., Fei, H., Prather, K. A. & Cohen, S. M. Postsynthetic ligand and cation exchange in robust metal-organic frameworks. *J. Am. Chem. Soc.* **134**, 18082–18088 (2012).
39. Lau, C. H., Babarao, R. & Hill, M. R. A route to drastic increase of CO_2 uptake in Zr metal organic framework UiO-66. *Chem. Commun.* **49**, 3634–3636 (2013).
40. Bon, V., Senkovskyy, V., Senkovska, I. & Kaskel, S. Zr(iv) and Hf(iv) based metal-organic frameworks with reo-topology. *Chem. Commun.* **48**, 8407–8409 (2012).
41. Yang, Q. *et al.* Probing the dynamics of CO_2 and CH4 within the porous zirconium terephthalate UiO-66(Zr): a synergic combination of neutron scattering measurements and molecular simulations. *Chemistry* **17**, 8882–8889 (2011).
42. Bushell, A. F. *et al.* Gas permeation parameters of mixed matrix membranes based on the polymer of intrinsic microporosity PIM-1 and the zeolitic imidazolate framework ZIF-8. *J. Membr. Sci.* **427**, 48–62 (2013).
43. Bae, T.-H. & Long, J. R. CO_2/N_2 separations with mixed-matrix membranes containing Mg2(dobdc) nanocrystals. *Energ. Environ. Sci.* 6, 3565–3569 (2013).
44. Perez, E. V., Balkus Jr, K. J., Ferraris, J. P. & Musselman, I. H. Mixed-matrix membranes containing MOF-5 for gas separations. *J. Membr. Sci.* **328**, 165–173 (2009).
45. Hill, R. J. Diffusive Permeability and Selectivity of Nanocomposite Membranes. *Ind. Eng. Chem. Res.* **45**, 6890–6898 (2006).
46. Creutz, C. & Chou, M. H. Binding of Catechols to Mononuclear Titanium(IV) and to 1- and 5-nm TiO2 Nanoparticles. *Inorg. Chem.* **47**, 3509–3514 (2008).
47. Lee, H. J., Koo, A. N., Lee, S. W., Lee, M. H. & Lee, S. C. Catechol-functionalized adhesive polymer nanoparticles for controlled local release of bone morphogenetic protein-2 from titanium surface. *J. Controlled Release* **170**, 198–208 (2013).
48. Chi, Y., Lan, J.-W., Ching, W.-L., Peng, S.-M. & Lee, G.-H. Syntheses and characterization of mixed acetylacetonate-catecholate complexes of zirconium, [Zr3(acac)4(cat)4(MeOH)2], [Zr(acac)2(DBcat)]2 (H2DBcat = 3,5-di-tert-butylcatechol) and [Zr4([small mu]4-O)(acac)4(DBcat)3(OMe)4(MeOH)]. *J. Chem. Soc., Dalton Trans.* **17**, 2923–2927 (2000).
49. Saxer, S. *et al.* Surface Assembly of Catechol-Functionalized Poly(l-lysine)-graft-poly(ethylene glycol) Copolymer on Titanium Exploiting Combined Electrostatically Driven Self-Organization and Biomimetic Strong Adhesion. *Macromolecules* **43**, 1050–1060 (2009).
50. Aslan, H., Eggers, S. H. & Dieter Fischer, R. Nitrile and isocyanide adducts of oxygen-bridged cationic biscyclopentadienyl titanium(IV) and zirconium(IV) fragments. *Inorg. Chim. Acta* **159**, 55–57 (1989).
51. Valenzano, L. *et al.* Disclosing the Complex Structure of UiO-66 Metal Organic Framework: A Synergic Combination of Experiment and Theory. *Chem. Mater.* **23**, 1700–1718 (2011).
52. Du, N., Song, J., Robertson, G. P., Pinnau, I. & Guiver, M. D. Linear High Molecular Weight Ladder Polymer via Fast Polycondensation of 5,5′,6,6′-Tetrahydroxy-3,3,3′,3′-tetramethylspirobisindane with 1,4-Dicyanotetrafluorobenzene. *Macromol. Rapid Commun.* **29**, 783–788 (2008).
53. Li, F. Y., Xiao, Y., Chung, T.-S. & Kawi, S. High-Performance Thermally Self-Cross-Linked Polymer of Intrinsic Microporosity (PIM-1) Membranes for Energy Development. *Macromolecules* **45**, 1427–1437 (2012).
54. Schaate, A. *et al.* Modulated Synthesis of Zr-Based Metal–Organic Frameworks: From Nano to Single Crystals. *Chem. Eur. J.* **17**, 6643–6651 (2011).

Acknowledgments

The authors would like to acknowledge Mark Greaves from the Electron Microscopy, Digital Imaging and Surface Analysis Facility within CSIRO for his contribution to this project. This research was supported by the Science and Industry Endowment Fund (SIEF).

Author contributions

S.J.D.S., C.H.L. and M.R.H. designed the experiments. S.J.D.S. carried out the experiments and characterization. C.H.L. and M.R.H. conceived the project. The manuscript was written by S.J.D.S. with contributions from C.H.L., M.R.H., B.P.L. and A.J.H. All authors have given approval to the final version of the manuscript.

Additional information

Supplementary information accompanies this paper at http://www.nature.com/scientificreports

Competing financial interests: The authors declare no competing financial interests.

How to cite this article: Smith, S.J.D., Ladewig, B.P., Hill, A.J., Lau, C.H. & Hill, M.R. Post-synthetic Ti Exchanged UiO-66 Metal-Organic Frameworks that Deliver Exceptional Gas Permeability in Mixed Matrix Membranes. *Sci. Rep.* **5**, 7823; DOI:10.1038/srep07823 (2015).